Journal of Engineering Mathematics 20 (1986) 127–144

The stability chart of double-diffusive processes with parallel flows – construction by the Galerkin and continuation methods

M. MAGEN, D. PNUELI and Y. ZVIRIN

Faculty of Mechanical Engineering, Technion, Israel Institute of Technology, Haifa 32000, Israel

(Received May 9, 1985 and in revised form October 15, 1985)

Summary

The stability of an infinite fluid layer subject to arbitrary horizontal flow and to arbitrary vertical temperature and salinity distributions is considered. Linear stability analysis is used to investigate the stability under general three-dimensional perturbations.

A general discussion of the properties of the stability chart, using only the governing equations, but not their solution for any particular case, is presented in [1]. This paper contributes a numerical scheme, based on a combination of the Galerkin and the continuation methods, to obtain the stability chart from the characteristic equation. The method is applied to an example with a parabolic velocity distribution and linear temperature and salinity fields. The stability chart in the plane of the Rayleigh numbers is obtained for the region corresponding to solar ponds.

1. Introduction

The stability of stratified flows appears in many geophysical processes and engineering applications, one of which is the solar pond, whose performance depends on maintaining its temperature and salinity distributions under horizontal flow conditions. Linear stability analysis of the flow with these three effects generally leads to an eigenvalue problem in which the operator is not self-adjoint. One effective way to handle such problems is the Galerkin method.

Ref. [1] * contains the derivation of the characteristic stability equation from the basic conservation equations, and also a discussion of some general properties of the stability chart. Magen [2] derived an approximate solution using the first-order Galerkin method. The present paper describes an accurate numerical method which utilizes the characteristic determinant of the problem and applies a combination of the Galerkin and continuation methods, e.g., Wasserstrom [3].

The application of the Galerkin method usually requires a solution of systems of algebraic equations, with matrices of high order. For example, Orszag [4] and Grosch and Salwen [5] solved the Orr-Sommerfeld equation by series with fifty, seventy, or a hundred terms. Thus, an accurate solution of the stability problem by the Galerkin method alone would require considerable computer time and a good-size memory. To reduce these, the continuation method is employed here, where the usual search for certain matrix parameters is replaced by numerical integration of a set of ordinary differential equations of first order.

* Ref. [1] also includes a summary of the relevant literature dealing with stability of double-diffusive systems with and without a horizontal flow, which is not repeated here.

The method is applied in detail to an example with a parabolic velocity distribution and linear vertical temperature and salinity profiles, and the stability chart is derived in the plane of the Rayleigh numbers. The boundary lines of the dynamic stability are found to be quite close to the statical stability margins (for a fluid at rest), when the Reynolds numbers are not too large ($\mathrm{Re} < 10^5$).

One of the most interesting processes of double-diffusive shear flows is that occurring in a solar pond. Utilization of solar energy by a solar pond is considered to have a potential for production of electricity and for low-grade heat applications [6–8]. The pond itself, which serves as both collector and storage, is typically $1 \div 2$ m deep and has an area of several hundreds or thousands square meters. The solar radiation is absorbed gradually in the water and the bottom layer is maintained at the higher temperature, typically about 90°C, while the temperature at the top is slightly above the ambient. The thermal Rayleigh number of the pond is of order 10^{13}, which would definitely create natural convection and mixing. In order to stabilize the pond, it is artificially stratified by salt, pouring layer over layer, each with a lower concentration. Thus, a continuous density distribution is achieved (due to diffusion). The salt concentration at the bottom is typically 30% or even reaches saturation, and at the top the density is just higher than that of fresh water.

The usual operation of the pond is by suction of the hot bottom layer, a process which is called "selective withdrawal", because the layers above it remain unmixed. The hot brine is circulated through a heat exchanger, either generating vapor of an organic fluid on the secondary side for driving a turbine-generator to produce electricity, or heating a secondary fluid which delivers the heat required.

The brine returns to the pond at a higher elevation than the outlet and on the other side, thus the heavier fluid settles back to its natural depth. Because of the strong stratification this process hardly causes any additional mixing. If the brine inlet is near the top, most of the shear flow in the pond has a velocity distribution which is nearly parabolic. Small regions beneath the inlet and above the outlet exhibit different flow patterns.

The stability chart is found here in a region of the Rayleigh numbers plane corresponding to solar ponds. From the results it can be deduced that the stability of a solar pond depends on the Reynolds number and that instability occurs when the order of magnitude of Re is larger than 10^4.

2. Analysis: statement of the problem – the governing equations

We consider an infinite fluid layer with an arbitrary horizontal flow and with arbitrary initial temperature and salinity gradients.

The governing equations for small perturbations superimposed on an undisturbed steady state have been derived in [1], starting from the equations of conservation of mass, momentum and energy. The variables were normalized, the equations were linearized and the pressure terms were eliminated to yield the following perturbation equations:

$$\begin{aligned}
&\left[D^2 - \beta^2 - \mathrm{i}\beta_x \,\mathrm{Re}\, P_j \mathring{u}(z)\right] T_j + D\mathring{T}_j(z) w = \sigma P_j T_j, \quad j = 1, 2; \\
&-\left\{\left(D^2 - \beta^2\right)^2 - \mathrm{i}\beta_x \,\mathrm{Re}\left[\mathring{u}(z)\left(D^2 - \beta^2\right) - D^2\mathring{u}(z)\right]\right\} w + \beta^2 (S_1 T_1 - S_2 T_2) \\
&\quad = -\sigma\left(D^2 - \beta^2\right) w
\end{aligned} \tag{1}$$

with the boundary conditions

$$w=0,\ D^2w=0:\quad \text{free boundary};\qquad w=0,\ Dw=0:\quad \text{rigid boundary};$$

$$DT_j + h_{uj}T_j=0:\text{upper boundary};\qquad -DT_j + h_{lj}T_j=0:\quad \text{lower boundary}, \tag{2}$$

where z and x are the coordinates in the vertical and flow directions, respectively, and y is perpendicular to both; also $D \equiv \mathrm{d}/\mathrm{d}z$. The perturbation of the vertical velocity component is assumed to have the form $w(z)\exp[\mathrm{i}(\beta_x x + \beta_y y) + \sigma t]$ where t is the time, σ is the stability parameter, β_x and β_y are wave numbers in the corresponding directions and $\beta^2 \equiv \beta_x^2 + \beta_y^2$. Similar expressions are assumed for the temperature and salinity perturbations, $T_1(z)$ and $T_2(z)$. $\mathring{u}$, $\mathring{T}_1$ and $\mathring{T}_2$ denote the undisturbed dimensionless velocity, temperature and salinity distributions. Re is the Reynolds number, defined by Q/ν where $Q = \int_0^d \mathring{u}(z)\mathrm{d}z$ (here $\mathring{u}(z)$ is the dimensional velocity) and d is a characteristic length (the depth of the flowing layer). $P_{1,2}$ are the Prandtl and Schmidt numbers, $P_j = \nu/K_j$, where ν is the kinematic viscosity and K_j $(j=1, 2)$ are the thermal and concentration diffusivities. The Rayleigh numbers for temperature and salinity are defined by $S_j = g\Delta T_j \alpha_j d^3/(\nu K_j)$ where g is the acceleration of gravity, ΔT_j are characteristic temperature and salinity differences and α_j are the respective expansion coefficients; h_{uj} and h_{lj} are Biot numbers for temperature and salinity.

The mathematical problem defined by Eqs. (1) and (2) is an eigenvalue (σ) and eigenfunctions (T_1, T_2, w) problem set by three ordinary differential equations with complex variable coefficients. This problem is not self-adjoint and therefore the stability parameter σ (eigenvalue) is generally complex. The stability criterion is:

$$\mathrm{Real}(\sigma) < 0 \tag{3}$$

for all the eigenvalues. For given $\mathring{u}(z)$, $\mathring{T}_1(z)$, $\mathring{T}_2(z)$, the flow is stable when the combination of the physical parameters of the problem (h_{lj}, h_{uj}, P_j, S_j, Re) guarantees that condition (3) is satisfied for every possible mode of small disturbance, i.e. for every wave number β and β_x in the range $0 \leqslant \beta < \infty$, $0 \leqslant \beta_x \leqslant \beta$.

The purpose of the present work is to derive the stability boundaries for general three-dimensional perturbations and to construct the stability chart in the Rayleigh-numbers plane (S_1, S_2). The first stage is to use the Squire transformation in order to obtain the chart for transverse two-dimensional perturbations (in the flow direction) for a fixed value of β. It is noted that the wave number in this direction (β_x) appears in the governing equations (1) only as a combination with the Reynolds number:

$$R \equiv \beta_x\ \mathrm{Re}. \tag{4}$$

The method outlined in [1] is then utilized to derive the general chart for three-dimensional disturbances and then to construct the envelope of the family of lines with β as a parameter. An accurate solution is presented here, based on the use of a general Galerkin technique.

3. Derivation of the characteristic equation by the Galerkin method

3.1. Choice of the trial functions

The Galerkin method requires the choice of complete sequences of trial functions which satisfy the boundary conditions (2). It is helpful to choose them particularly related to the operators of the governing equations (1). We thus choose the trial functions ϕ_j ($j = 1, 2, 3$ for temperature, salinity and velocity) as the solutions of the following equations and boundary conditions:

$$\begin{aligned} &(D^2 - \beta^2)\phi_j + \lambda_j^2 \phi_j = 0, \\ &D\phi_j - h_{lj}\phi_j \,|_{z=0} = D\phi_j + h_{uj}\phi_j \,|_{z=1} = 0, \quad j = 1, 2; \end{aligned} \tag{5}$$

$$-(D^2 - \beta^2)^2 \phi_3 - \lambda_3^2 (D^2 - \beta^2)\phi_3 = 0,$$

$$\text{on rigid boundary: } \phi_3 = 0,\ D\phi_3 = 0, \tag{6}$$

$$\text{on free boundary: } \phi_3 = 0,\ D^2\phi_3 = 0.$$

Equations (5) and (6) constitute rather simple problems to find the eigenvalues λ_j and eigenfunctions $\phi_j(z)$. A solution of Eq. (6) appears, for example, in Harris and Reid [9]. Furthermore, the eigenfunctions $\phi_j(z)$ may be normalized to satisfy the orthonormal conditions

$$\begin{aligned} &\langle \phi_{jm} \cdot \phi_{jn} \rangle = \delta_{mn} \rightarrow \langle \phi_{jm} \cdot (D^2 - \beta^2)\phi_{jn} \rangle = -\lambda_{jm}^2 \delta_{mn}, \\ &\langle \phi_{3m} \cdot (\beta^2 - D^2)\phi_{3n} \rangle = \delta_{mn} \rightarrow -\langle \phi_{3m} \cdot (D^2 - \beta^2)^2 \phi_{3n} \rangle = -\lambda_{3m}^2 \delta_{mn}, \\ &j = 1, 2;\ m, n = 1, 2, 3, \ldots, \end{aligned} \tag{7}$$

where $\langle \ldots \rangle \equiv \int_0^1 \ldots \mathrm{d}z$.

3.2. Derivation of the characteristic equation

The eigenfunctions of Eq. (1) can be expanded as a series in the complete sequences of the trial functions satisfying Eqs. (5) and (6). Truncation of the series after the first N terms defines the Nth-order Galerkin approximation

$$T_j \cong \sum_{n=1}^{N} C_{jn}\phi_{jn}(z), \quad w \cong \sum_{n=1}^{N} C_{3n}\phi_{3n}(z), \quad j = 1, 2, \quad C_{in} = \text{constant}. \tag{8}$$

The finite series (8) satisfy the boundary conditions (2), but they do not generally satisfy the differential equations of the problem (1).

Eqs. (8) are now substituted into Eqs. (1), and we require that:
- the residue of the first of Eq. (1) be orthogonal to all eigenfunctions $\phi_{1n}(z)$, $n = 1, 2 \ldots N$;
- the residue of the second of Eq. (1) be orthogonal to $\phi_{2n}(z)$;
- the residue of the third of Eq. (1) be orthogonal to $\phi_{3n}(z)$.

These operations result in:

$$[A]\{C\} = 0 \tag{9}$$

where the eigenvector-column C includes the $3N$ coefficients C_{in} of the expansions (8) and A is a square complex $3N \times 3N$ matrix. Eq. (9) is homogeneous and the determinant of A must vanish. The characteristic equation for the stability parameter σ may therefore be written in the following form:

$$\Delta_{3N} = |A| = \begin{vmatrix} -\Lambda_1 - P_1\sigma I - \mathrm{i}RP_1\Gamma_1 & 0 & \eta_1 \\ 0 & -\Lambda_2 - P_2\sigma I - \mathrm{i}RP_2\Gamma_2 & \eta_2 \\ S_1\beta^2\nu_1 & -S_2\beta^2\nu_2 & -\Lambda_3 - \sigma I - \mathrm{i}R\Gamma_3 \end{vmatrix} = 0 \tag{10}$$

where I, Λ_i, Γ_j, ν_j, η_j are square real $N \times N$ matrices, defined as:

$$\begin{aligned} &[I]_{mn} = \delta_{mn}, \quad [\Lambda_i]_{mn} = \lambda_{im}^2\delta_{mn}, \quad [\nu_j]_{mn} = \langle \phi_{3m} \cdot \phi_{jn} \rangle, \\ &[\eta_j]_{mn} = \langle \phi_{jm} \cdot D\mathring{T}_j\phi_{3n} \rangle, \quad [\Gamma_j]_{mn} = \langle \phi_{jm} \cdot \mathring{u}\phi_{jn} \rangle, \\ &[\Gamma_3]_{mn} = \langle \phi_{3m} \cdot [\mathring{u}(D^2 - \beta^2) - D^2\mathring{u}]\phi_{3n} \rangle, \\ &j = 1, 2; \; i = 1, 2, 3; \; m, n = 1, 2 \ldots N. \end{aligned} \tag{11}$$

To obtain the form (10) of the characteristic determinant Δ_{3N}, the conditions of orthonormality (7) must also be used.

It is noted that the matrices Γ, ν, η, Λ depend on the boundary conditions (2), on the shape of the undisturbed distributions $\mathring{T}_1(z)$, $\mathring{T}_2(z)$, $\mathring{u}(z)$ and on the wave number β. However, they are independent of the physical parameters S_j, P_j, Re and the stability parameter σ. Thus one may treat the characteristic determinant Δ_{3N} either as a polynomial of degree $3N$ in σ or R, or as a polynomial of degree N in S_1 or S_2. The stability condition (3) requires that all the roots σ of the polynomial have non-positive real part. In principle, it is possible to derive some analytical conditions for this requirement (Real(σ) $\leqslant 0$). This has been done by Magen [2] for $N = 1$. However, for $N \geqslant 2$, an analytical derivation of the necessary conditions is practically impossible and a numerical method must be employed.

3.3. Modifications of the characteristic determinant

To simplify the numerical calculations, the form of the determinant Δ_{3N} in the characteristic equation (10) is modified. The first column of Δ_{3N} is multiplied by P_1^{-1} and the second column by P_2^{-1}. Eq. (10) can now be rewritten as

$$\sigma = \text{E.V.}\begin{bmatrix} -\Lambda_1/P_1 - \mathrm{i}R\Gamma_1 & 0 & \eta_1 \\ 0 & -\Lambda_2/P_2 - \mathrm{i}R\Gamma_2 & \eta_2 \\ (S_1\beta^2/P_1)\nu_1 & -(S_2\beta^2/P_2)\nu_2 & -\Lambda_3 - \mathrm{i}R\Gamma_3 \end{bmatrix} \tag{12}$$

and σ is expressed as the eigenvalue of the square $3N \times 3N$ matrix. Another modification is now performed on the determinant. First, it is noted that the value of Δ_{3N} will remain zero when its matrix is multiplied by another matrix $\tilde{I}$, with a unit determinant. Let this other matrix be defined as

$$\tilde{I} = \left[\begin{array}{c|c|c} I & 0 & 0 \\ \hline 0 & I & 0 \\ \hline \beta^2 S_1 \nu_1 \cdot (\Lambda_1 + P_1 \sigma I + \mathrm{i} R P_1 \Gamma_1)^{-1} & -\beta^2 S_2 \nu_2 \cdot (\Lambda_2 + P_2 \sigma I + \mathrm{i} R P_2 \Gamma_2)^{-1} & I \end{array}\right], \tag{13}$$

and let it be multiplied from the left by the matrix of Δ_{3N}. This leads to a determinant with zero blocks beneath the principal diagonal, whose value is given by the product of the determinants of the blocks in this diagonal. After some manipulations a $N \times N$ determinant is obtained, and the characteristic equation reduces to

$$\Delta_N = |\beta^2 S_1 \nu_1 \cdot (\Lambda_1 + P_1 \sigma I + \mathrm{i} R P_1 \Gamma_1)^{-1} \cdot \eta_1 - \beta^2 S_2 \nu_2 \cdot (\Lambda_2 + P_2 \sigma I + \mathrm{i} R P_2 \Gamma_2)^{-1} \cdot \eta_2 - \Lambda_3 - \sigma I - \mathrm{i} R \Gamma_3| = 0. \tag{14}$$

A necessary condition for this derivation is *

$$|\Lambda_j + P_j \sigma I + \mathrm{i} R P_j \Gamma_j| \neq 0, \quad j = 1, 2. \tag{15}$$

Eq. (14) can be considered as a generalized eigenvalue problem for S_1 or for S_2 as the eigenvalues. For example, multiplying the matrix of Eq. (14) on the left by the matrix $\beta^{-2} \eta_1^{-1} \cdot (\Lambda_1 + P_1 \sigma I + \mathrm{i} R P_1 \Gamma_1) \cdot \nu_1^{-1}$ leads, for $|\nu_1| \neq 0$, $|\eta_1| \neq 0$, to the following formal representation:

$$\begin{aligned} S_{1c} &= S_{1r} + \mathrm{i}\xi \\ &= \text{E.V.}\{\eta_1^{-1} \cdot (\Lambda_1 + P_1 \sigma I + \mathrm{i} R P_1 \Gamma_1) \cdot \nu_1^{-1} \cdot (S_2 \nu_2 \cdot (\Lambda_2 + P_2 \sigma I + \mathrm{i} R P_2 \Gamma_2)^{-1} \cdot \eta_2 \\ &\quad + \beta^{-2}(\Lambda_3 + \sigma I + \mathrm{i} R \Gamma_3))\}. \end{aligned} \tag{16}$$

The marginal stability curves, where $\text{Real}(\sigma) = 0$ and

$$\sigma = \mathrm{i}\omega, \tag{17}$$

will be derived from the characteristic Eq. (14) or (16). In general, the right-hand side of Eq. (16) is a complex, non-Hermitian matrix and S_{1c} has a complex value. However, since S_1 (on the left-hand side) is real, the marginal stability lines are defined by the set of parameters ω, R and S_2 for which the imaginary part of one of the eigenvalues is zero ($\xi = 0$) and its real part (S_{1r}) equals S_1. This procedure yields an eigenvalue σ with $\text{Real}(\sigma) = 0$ for the matrix (12), but it is still necessary to check whether the other eigenvalues of this matrix satisfy condition (3) (have negative real parts).

* This condition has been derived by Magen [2] for the marginal stability lines, i.e. $\text{Real}(\sigma) = 0$; ref. [2] also includes additional details of the mathematical treatment.

The derivation of the stability chart from Eq. (12) would be quite lengthy and it is easier to obtain the eigenvalues from Eqs. (16,17), but some additional checks must then be performed. An "optimal" numerical method which is a combination of both approaches is developed here.

3.4. The characteristic equation for a special case

In order to demonstrate the application of the procedure outlined above we consider the case of linear temperature and salinity distributions $\mathring{T}_{1,2}(z)$ with identical boundary conditions for both, i.e.:

$$D\mathring{T}_j(z) \equiv 1, \quad h_{ju} = h_u, \quad h_{jl} = h_l, \quad j = 1, 2. \tag{18}$$

As can be seen from Eqs. (5) and (6), $\phi_{1m} = \phi_{2m}$ in this case. Substitution of Eq. (18) into (7) and (11) yields

$$\Lambda_1 = \Lambda_2 = \Lambda, \quad \Gamma_1 = \Gamma_2 = \Gamma, \quad \eta_1 = \eta_2 = \eta, \quad \nu_1 = \nu_2 = \eta^T, \tag{18a}$$

and the characteristic equations (12) and (16) reduce to

$$\sigma = \text{E.V.}\left[\begin{array}{c|c|c} -\Lambda/P_1 - \mathrm{i}R\Gamma & 0 & \eta \\ \hline 0 & -\Lambda/P_2 - \mathrm{i}R\Gamma & \eta \\ \hline (S_1\beta^2/P_1)\eta^T & -(S_2\beta^2/P_2)\eta^T & -\Lambda_3 - \mathrm{i}R\Gamma_3 \end{array}\right], \tag{19}$$

$$\begin{aligned} S_{1c} &= S_{1r} + \mathrm{i}\xi \\ &= \text{E.V.}\Big\{(\Lambda + P_1\sigma I + \mathrm{i}RP_1\Gamma)\cdot\Big[S_2(\Lambda + P_2\sigma I + \mathrm{i}RP_2\Gamma)^{-1} \\ &\qquad + \beta^{-2}(\eta^T)^{-1}\cdot(\Lambda_3 + \sigma I + \mathrm{i}R\Gamma_3)\cdot\eta^{-1}\Big]\Big\}. \end{aligned} \tag{20}$$

For the static stability case (of the rest state, $\mathrm{Re} = R = 0$), the determinant in Eq. (14) takes the form

$$\Delta_N \mid_{R=0} = \left|\beta^2\eta^T\cdot\Lambda_0\cdot\eta - \Lambda_3 - \sigma I\right|$$

where

$$[\Lambda_0]_{mn} = \frac{(S_1 - S_2)\lambda_m^2 + \sigma(S_1P_2 - S_2P_1)}{(\lambda_m^2 + P_1\sigma)(\lambda_m^2 + P_2\sigma)}\delta_{mn}. \tag{21}$$

From Eq. (21) it is possible to obtain the following condition for monotonic instability (i.e. $\sigma = 0$), for a specific value of the wave number β:

$$S_1 - S_2 = S_N(\beta) = \beta - 2\ \text{min E.V.}\left[\Lambda^{1/2}\cdot(\eta^T)^{-1}\cdot\Lambda_3\eta^{-1}\cdot\Lambda^{1/2}\right] \tag{22}$$

where $[\Lambda^{1/2}]_{mn} = \lambda_m \delta_{mn}$. The matrix in the last equation is symmetric and positive definite, hence all its eigenvalues are real and positive.

The static marginal stability line for all possible modes β can be found by rewriting Eq. (22) in the form

$$S_1 - S_2 = S^* = \lim_{N \to \infty} \min_{\beta} S_N(\beta), \tag{23}$$

which represents a straight line in the S_1, S_2 plane. This result has also been obtained by Nield [10], who calculated critical values of S^* for various boundary conditions.

The following analysis is based on the simplified equations (19) and (20); however, the same procedure can be applied to more general cases, using Eqs. (12) and (16).

4. Numerical derivation of the stability chart

Two numerical methods are used in the present work to find the eigenvalues: the QR method and the VI method, c.f. Wilkinson [11]. The first (QR) transforms the given matrix to an equivalent triangular form with the same eigenvalues. The method then yields simultaneously all the eigenvalues without any exceptions, even when several eigenvalues are equal or nearly equal. However, this method becomes quite expensive for large N.

The second method, "vector iterations with shift" (VI), converges to the eigenvector and eigenvalue nearest to an initial guess. It is considerably less expensive than the previous one, but only one eigenvalue at a time is obtained, and its convergence may be very slow or even fail in cases of repeated or close eigenvalues.

In what follows two different problems must be solved. The first problem is to find a first point somewhere on the stability boundary curve. The second problem is to find a point on the stability boundary in the neighborhood of a known point. In both problems an ordered search is conducted for the values of some parameters, which yields real or imaginary eigenvalues. For this, use has been made of the "continuation method", c.f. Wasserstrom [3], where instead of an arbitrary search, the solution is obtained by the numerical integration of a set of first-order ordinary differential equations.

4.1. First problem: find a first point on the stability boundary curve

For given values of S_2, Re and β, we choose the value S_{10} as a first approximation (guess) for S_1. The QR method is used to obtain all the $3N$ eigenvalues of Eq. (19). The eigenvalue with the largest real part is denoted by $\sigma_0 = \psi_0 + i\omega_0$. In general, $\psi_0 \neq 0$ and a search is begun to find the value of S_1 which corresponds to $\psi = \text{Real}(\sigma) = 0$. This search is conducted by the continuation method, i.e., by the solution of the ordinary differential equations

$$\frac{dS_1}{d\psi} = \left\{ \text{Real}\left[(\partial S_{1c}/\partial\sigma)^{-1} \right] \right\}^{-1}, \quad \frac{d\omega}{d\psi} = -\frac{\text{Im}(\partial S_{1c}/\partial\sigma)}{\text{Real}(\partial S_{1c}/\partial\sigma)} \tag{24}$$

with the initial conditions $S_1(\psi_0) = S_{10}$, $\omega(\psi_0) = \omega_0$. Any convenient form of numerical

integration may be used, and we have employed the simple Euler method. For the first step, new values for S_1 and ω are calculated from Eq. (24) by the approximation

$$\begin{aligned} S_{11} &= S_{10} + \Delta\psi \,|\, \partial S_{1c}/\partial\sigma \,|^2 / \mathrm{Real}(\partial S_{1c}/\partial\sigma) + \mathrm{O}(\Delta\psi)^2, \\ \omega_1 &= \omega_0 - \Delta\psi \ \mathrm{Im}(\partial S_{1c}/\partial\sigma)/\mathrm{Real}(\partial S_{1c}/\partial\sigma) + \mathrm{O}(\Delta\psi)^2, \\ \psi_1 &= \psi_0 + \Delta\psi, \end{aligned} \tag{25}$$

where the derivative $\partial S_{1c}/\partial\sigma$ is obtained from Eq. (A-4) of Appendix A by the VI method. The requirement $\mathrm{Im}(S_{1c}) = 0$ has been satisfied in the derivation of Eqs. (25). The change in $\mathrm{Real}(\sigma)$ (i.e. $\Delta\psi$) is chosen small enough and the integration is continued until convergence to $\psi = 0$ is achieved. The value found for S_1 defines a point on the marginal stability line for the given S_2, Re and β.

4.2. Second problem: find a point on the stability boundary near a known point

Consider the situation where a point on the marginal stability line has already been found. Denote the parameters of this point by S_{10}, S_{20}, ω_0, R. We seek now another point on this marginal stability curve for a different given value of S_2 (say S_{21}), but for the same value of R. The values of S_1 and ω for the new point, S_{11} and ω_1, can be found, again, by the continuation method. The ordinary differential equations

$$\frac{\mathrm{d}\omega}{\mathrm{d}S_2} = -\frac{\mathrm{Im}(\partial S_{1c}/\partial S_2)}{\mathrm{Im}(\partial S_{1c}/\partial\omega)}, \quad \frac{\mathrm{d}S_1}{\mathrm{d}S_2} = \mathrm{Real}\frac{\partial S_{1c}}{\partial S_2} + \frac{\mathrm{d}\omega}{\mathrm{d}S_2}\mathrm{Real}\frac{\partial S_{1c}}{\partial\omega} \tag{26}$$

are integrated numerically, starting from $S_1(S_{20}) = S_{10}$. The new values of S_1 and ω after the first step are given by

$$\begin{aligned} \omega_1 &= \omega_0 + \Delta\omega = \omega_0 - \Delta S_2 \ \mathrm{Im}(\partial S_{1c}/\partial S_2)/\mathrm{Im}(\partial S_{1c}/\partial\omega), \\ S_{11} &= S_{10} + \Delta S_2 \ \mathrm{Real}(\partial S_{1c}/\partial S_2) + \Delta\omega \ \mathrm{Real}(\partial S_{1c}/\partial\omega), \end{aligned} \tag{27}$$

where the derivatives $\partial S_{1c}/\partial S_2$ and $\partial S_{1c}/\partial\omega$ are taken from Eqs. (A-3, A-5) of Appendix A. Again, the requirement $\mathrm{Im}(S_{1c}) = 0$ has been satisfied in the derivation of Eqs. (27).

In general, the introduction of R, $S_{21} = S_{20} + \Delta S_2$ and ω_1 into Eq. (20) does not lead to an exact eigenvalue (with zero imaginary part and a real part equal to S_{11}). Keeping S_2 unchanged we iterate to improve the values of S_{1c}. To do this we use the VI method to solve Eq. (20), and then modify the resulting approximation S_{1i} by changing ω such that $\mathrm{Im}(S_{1ci}) = 0$. The procedure is repeated until convergence to a satisfactory value of S_1 is achieved.

The goal of the numerical methods just outlined is to reduce the lengthy computations of the eigenvalues σ (Eq. 19) required by the QR method, which is therefore used only once, to obtain the first point on the stability boundary (Section 4.1). Care must be taken, however, to locate the true marginal curve in the stability chart; if $\Delta\psi$ (method 4.1) or ΔS_2 (method 4.2) are too large, the calculations might converge to a point on a line segment where still $\mathrm{Real}(\sigma) = 0$, but there exists another eigenvalue $\tilde{\sigma}$ (for the same parameters) with $\mathrm{Real}(\tilde{\sigma}) > 0$.

5. Construction of the stability chart for a special case

As an illustration consider the following example: an infinite fluid layer has a rigid bottom boundary and a free surface at the top. The values of the temperature and the salinity are fixed at the top and at the bottom boundaries, and the initial undisturbed distributions are

$$\mathring{u}(z) = 1.5(2z - z^2), \quad DT_j(z) \equiv 1, \quad h_l = h_u = \infty. \tag{28}$$

Equations (5)–(7) yield, then, the following expressions for the trial functions:

$$\begin{aligned} &\phi_{1m} = \phi_{2m} = \phi_m(z) = \sqrt{2}\sin m\pi z, \\ &\lambda_{1m}^2 = \lambda_{2m}^2 = \lambda_m^2 = m^2\pi^2 + \beta^2, \end{aligned} \tag{29}$$

$$\begin{aligned} &\phi_{3m}(z) = \sqrt{\frac{2}{(\beta^2+\mu_m^2)(1+\beta_t/\mu_m^2)}}\left[\frac{\sin\mu_m(1-z)}{\sin\mu_m} - \frac{\sinh\beta(1-z)}{\sinh\beta}\right], \\ &\beta_t \equiv \frac{\beta}{\tanh\beta}\left(\frac{\beta}{\tanh\beta} - 1\right), \quad \lambda_{3m}^2 = \mu_m^2 + \beta^2, \quad \frac{\tan\mu}{\mu} = \frac{\tanh\beta}{\beta}. \end{aligned} \tag{30}$$

Substitution of Eqs. (29)–(30) into (11) and integrations yield (see also Eq. (18a))

$$[\Lambda]_{mn} = (\pi^2 m^2 + \beta^2)\delta_{mn}, \quad [\Lambda_3]_{mn} = (\mu_m^2 + \beta^2)\delta_{mn},$$

$$[\Gamma]_{mm} = 1 + \frac{3}{4m^2\pi^2}, \quad [\Gamma]_{mn} = -\frac{12mn}{(m^2-n^2)^2\pi^2},$$

$$\begin{aligned} [\Gamma_3]_{mm} = \Bigg\{ &3\left(\frac{\beta_t}{\beta^2} - 1\right) - 3\left(\frac{\beta_t}{\mu_m^2} + 1\right) + 6\frac{2\beta_t + \mu_m^2 - \beta^2}{\mu_m^2 + \beta^2} \\ &+ \frac{\mu_m^2 + \beta^2}{4\mu_m^2}\left[1 + \frac{\beta^2}{\mu_m^2\tanh^2\beta} + \frac{3}{4\mu_m^2}\left(\frac{\beta_t}{\mu_m^2} - 1\right)\right]\Bigg\} \Big/ (\beta^2 + \mu_m^2)\left(1 + \frac{\beta_t}{\mu_m^2}\right), \end{aligned} \tag{31}$$

$$\begin{aligned} [\Gamma_3]_{mn} = &\left[3\left(\frac{\beta_t}{\beta^2} - 1\right) - 6(\mu_n^2 + \beta^2)\frac{2\beta_t + \mu_m^2 + \mu_n^2}{(\mu_m^2 - \mu_m^2)^2} + 6\frac{2\beta_t + \mu_m^2 - \beta^2}{\mu_n^2 + \beta^2}\right] \\ &/\left[(\beta^2 + \mu_m^2)(\beta^2 + \mu_n^2)/(1 + \beta_t/\mu_m^2)(1 + \beta_t/\mu_n^2)\right]^{1/2}, \end{aligned}$$

$$[\eta]_{mn} = \frac{2mn}{m^2\pi^2 + \beta^2}\frac{1}{m^2\pi^2 - \mu_n^2}\sqrt{\frac{\beta^2 + \mu_n^2}{1 + \beta_t/\mu_n^2}}.$$

In this case the inverse matrix η^{-1} can be found analytically, c.f. Magen [2],

$$[\eta^{-1}]_{mn} = \sqrt{\frac{1+\beta_t/\mu_m^2}{\beta^2+\mu_m^2}} \frac{\prod_{k=1}^{N}(\pi^2k^2-\mu_m^2)}{\prod_{k=1,k\neq m}^{N}(\mu_k^2-\mu_m^2)} \frac{1}{\pi^2n^2-\mu_m^2}$$

$$\times \frac{\prod_{k=1}^{N}(\pi^2n^2-\mu_k^2)}{\prod_{k=1,k\neq n}(n^2\pi^2-\pi^2k^2)} \frac{2\pi n}{n^2\pi^2+\beta^2}. \tag{32}$$

All the matrices in Eqs. (19), (20) have now been specified and the numerical derivation of the stability boundary may commence.

5.1. Static stability margins

It is well known, c.f. Nield [10], that the static stability boundary (of the rest state, $\mathrm{Re} = 0$) in the S_1, S_2 plane consists of two curves: a monotonic stability line (on which $\sigma = 0$) and an oscillatory stability line (on which $\mathrm{Real}(\sigma) = 0$, but $\mathrm{Im}(\sigma) \neq 0$).

In the special case when the temperature and the salinity have identical dimensionless boundary conditions and initial distributions, the monotonic stability curve is a straight line with a 45° slope, i.e. $S_1 - S_2 = S_N(\beta)$. If, in addition, the initial distributions of $T_{1,2}$ are linear, $S_N(\beta)$ can be found from Eq. (22). This has been done here for various values of N and β, with the results (see Eq. (23)) $S^* = 1100.657$ for $\beta^* = 2.683$. These values are well known; Reid and Harris [9], for example, obtained the same results by a different method. The monotonic static stability line is, thus, completely defined.

A simple analytical form of the oscillatory static stability curve is not known and it must be found numerically. The results of the numerical method, described in Section 4 above, are summarized in Table 1 *: S_1 on this line is given, together with the corresponding frequency ω, as functions of S_2, for various values of β. A first approximation for this curve, obtained in [2], is a straight line, which moves and rotates with changes of β. It can be seen that indeed the curve can be approximated by the straight line

$$S_1 - S_{1\min}(\beta, N) = K(\beta, N)[S_2 - S_{2\min}(\beta, N)]. \tag{33}$$

The point $S_{1\min}$, $S_{2\min}$ is the intersection of the monotonic and oscillatory stability lines, see also Eq. (22). The values of $K(\beta)$, listed in Table 2, have been obtained by fitting the straight line (33) to the numerical values. From these results an approximate expression has been derived for $\omega = \mathrm{Im}(\sigma)$ on the oscillatory stability line

$$\omega = [a_\omega(\beta, N)(S_2/S_{2\min} - 1)]^{1/2}. \tag{34}$$

Table 2 includes the values of S_N, K, $S_{1\min}$, $S_{2\min}$ and a_ω for various values of β. The results of the approximations (33) and (34), as well as the results of the first-order

* Table 1 includes, as an example, only two values of the wave number β. Additional results appear in [2].

Table 1. A comparison of three methods for finding points on a static oscillatory marginal-stability curve for various values of the wave number β: thermal Rayleigh number S_1 and perturbation frequency ω for various values of the saline Rayleigh number S_2. The methods are, respectively: (i) an exact numerical method based on Galerkin, (ii) the approximate formula (33) based on Galerkin, and (iii) a first-order approximation of the Galerkin method, [2].

$\beta = 0.5181\text{E}-01$

S_2	Exact value		Approximate formula (33)		First-order approximation	
	S_1	ω	S_1	ω	S_1	ω
0.1016E+05	0.9145E+06	0.2839E−02	0.9145E+06	0.2839E−02	0.9771E+06	0.0
0.1045E+05	0.9145E+06	0.3779E−02	0.9145E+06	0.3864E−02	0.9771E+06	0.5024E−03
0.1077E+05	0.9145E+06	0.4550E−02	0.9145E+06	0.4693E−02	0.9771E+06	0.2496E−02
0.1956E+05	0.9147E+06	0.1416E−01	0.9146E+06	0.1484E−01	0.9772E+06	0.1317E−01
0.5317E+05	0.9152E+06	0.2989E−01	0.9149E+06	0.3129E−01	0.9775E+06	0.2852E−01
0.7825E+05	0.9155E+06	0.3760E−01	0.9152E+06	0.3931E−01	0.9778E+06	0.3593E−01
0.2624E+06	0.9177E+06	0.7261E−01	0.9169E+06	0.7552E−01	0.9795E+06	0.6927E−01
0.1296E+07	0.9280E+06	0.1646E+00	0.9268E+06	0.1704E+00	0.9892E+06	0.1564E+00
0.6399E+07	0.9776E+06	0.3677E+00	0.9753E+06	0.3978E+00	0.1037E+07	0.3488E+00
0.3171E+08	0.1222E+07	0.8200E+00	0.1216E+07	0.8459E+00	0.1274E+07	0.7768E+00
0.1524E+09	0.2387E+07	0.1805E+01	0.2365E+07	0.1855E+01	0.2403E+07	0.1703E+01
0.1593E+09	0.2454E+07	0.1846E+01	0.2431E+07	0.1896E+01	0.2467E+07	0.1742E+01
0.7665E+09	0.8258E+07	0.4111E+01	0.8209E+07	0.4160E+01	0.8147E+07	0.3820E+01
0.1010E+10	0.1057E+08	0.4743E+01	0.1053E+08	0.4775E+01	0.1043E+08	0.4386E+01
0.1432E+10	0.1454E+08	0.5686E+01	0.1454E+08	0.5686E+01	0.1437E+08	0.5222E+01

$\beta = 0.5177\text{E}+02$

S_2	Exact value		Approximate formula (33)		First-order approximation	
	S_1	ω	S_1	ω	S_1	ω
0.8638E+05	0.7348E+07	0.6656E+00	0.7348E+07	0.6656E+00	0.7355E+07	0.6551E+00
0.8897E+05	0.7348E+07	0.9483E+00	0.7348E+07	0.9483E+00	0.7355E+07	0.9407E+00
0.9164E+05	0.7348E+07	0.1170E+01	0.7348E+07	0.1170E+01	0.7355E+07	0.1164E+01
0.1677E+06	0.7349E+07	0.3842E+01	0.7349E+07	0.3843E+01	0.7356E+07	0.3839E+01
0.4737E+06	0.7352E+07	0.8285E+01	0.7352E+07	0.8285E+01	0.7358E+07	0.8280E+01
0.6709E+06	0.7353E+07	0.1017E+02	0.7353E+07	0.1017E+02	0.7360E+07	0.1016E+02
0.2449E+07	0.7369E+07	0.2041E+02	0.7369E+07	0.2041E+02	0.7376E+07	0.2040E+02
0.1266E+08	0.7458E+07	0.4706E+02	0.7458E+07	0.4706E+02	0.7465E+07	0.4703E+02
0.6545E+08	0.7921E+07	0.1073E+03	0.7921E+07	0.1073E+03	0.7928E+07	0.1072E+03
0.3383E+09	0.1031E+08	0.2440E+03	0.1031E+08	0.2440E+03	0.1032E+08	0.2439E+03
0.1749E+10	0.2268E+08	0.5549E+03	0.2268E+08	0.5549E+03	0.2268E+08	0.5547E+03
0.8382E+10	0.8080E+08	0.1215E+04	0.8080E+08	0.1215E+04	0.8081E+08	0.1214E+04
0.9042E+10	0.8658E+08	0.1262E+04	0.8658E+08	0.1262E+04	0.8659E+08	0.1261E+04
0.1377E+11	0.1280E+09	0.1557E+04	0.1280E+09	0.1557E+04	0.1280E+09	0.1556E+04
0.2794E+11	0.2521E+09	0.2218E+04	0.2521E+09	0.2218E+04	0.2521E+09	0.2217E+04

Galerkin method ($N = 1$), obtained by Magen [2], are compared in Table 1 with the exact numerical solution. The agreement is quite good, justifying the use of the first-order method ($N = 1$) in this case.

Using Table 1, it is possible to draw the family of the oscillatory stability lines with β as a parameter, and then to trace its envelope. The complete static stability boundary can thus be obtained.

Table 2 shows that the slope K of the line (33) is almost independent of β while S_N, $S_{1\min}$ and $S_{2\min}$ strongly depend on it. Therefore, a change in β causes significant

Table 2. Parameters of monotonous and oscillatory static marginal-stability lines, Eqs. (33), (34), for various values of the wave number β.

β	Λ	K	$S_{2\min}$	$S_{1\min}$	K_ω
0.51816E−01	0.90476E+06	0.93929E−02	0.91452E+06	0.97603E+04	0.22119E−03
0.13899E+00	0.12616E+06	0.93915E−02	0.12752E+06	0.13611E+04	0.22192E−03
0.37281E+00	0.17949E+05	0.93817E−02	0.18143E+05	0.19378E+03	0.22722E−03
0.10000E+01	0.29381E+04	0.93170E−02	0.29699E+04	0.31864E+02	0.24112E−03
0.26823E+01	0.11007E+04	0.90479E−02	0.11130E+04	0.12222E+02	0.59428E−03
0.71949E+01	0.48584E+04	0.87993E−02	0.49141E+04	0.55736E+02	0.78905E−02
0.19299E+02	0.15072E+06	0.87645E−02	0.15246E+06	0.17392E+04	0.29870E+00
0.51766E+02	0.72644E+07	0.87626E−02	0.73483E+07	0.83859E+05	0.14765E+02

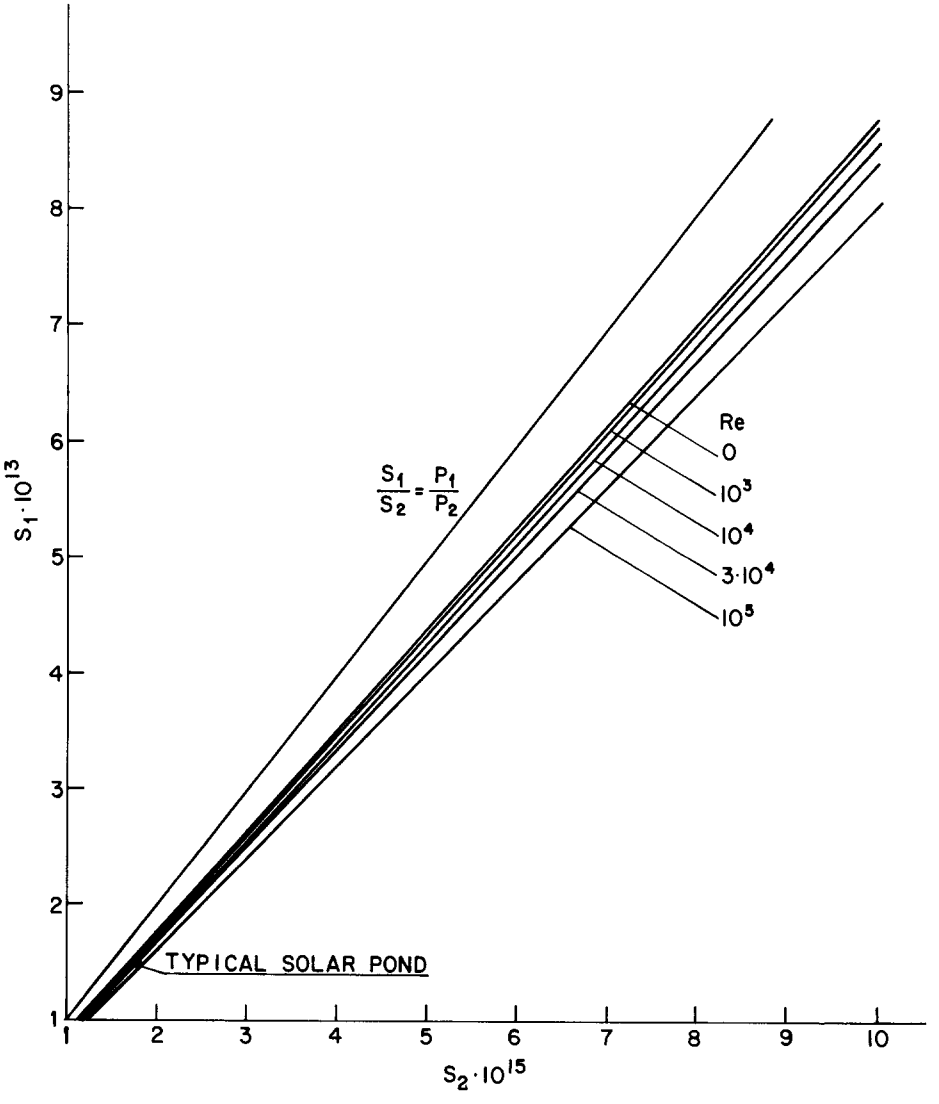

Figure 1. Exact marginal stability lines for various values of Re in the Rayleigh-numbers plane (S_1, S_2), obtained by the Galerkin method.

translation and small rotation of the line. A graphical tracing of the envelope here would be rather difficult, but it can be done numerically by finding the minimal value of $S_1(\beta)$ for any value of S_2. In the range $S_2 < 10^5$, the value of S_1 on the static oscillatory stability boundary is dominated by $S_{1\min}$ (see Tables 1 and 2). Therefore, the most dangerous perturbation in this region has the wave number $\beta \cong \beta^* = 2.68$. For large S_2 ($S_2 > 10^{10}$), however, S_1 is dominated by the product $S_2 K(\beta)$, and the critical perturbation has $\beta = 50 \div 60$.

The stability chart for the range $S_2 = 10^{15} \div 10^{16}$, corresponding to a typical solar pond, is shown in Figure 1. The chart includes the oscillatory static marginal stability line (Re = 0) as well as the dynamic stability boundaries for various values of Re (obtained as explained in the next section). The chart corresponds to $\beta = 20\beta^* = 53.6$; the numerical calculations show that variations of β between 50 and 60 change the value of S_1 by less than 0.1%.

The monotonic static stability margin almost coincides with the S_1 axis in Fig. 1, clearly in the unstable zone for oscillatory disturbances. The region where monotonic perturbations are the most dangerous is located near the origin in the $S_1 - S_2$ plane, not shown in Fig. 1. More details of these lines, obtained by the first-order Galerkin technique, are given by Magen [2].

5.2. Dynamic stability margins

As mentioned above, Fig. 1 includes dynamic marginal stability lines for various values of the Reynolds number Re. All these lines have been obtained for transverse two-dimensional perturbations, i.e. $\beta_x = \beta$. The numerical calculations show that in the case considered here the condition $\partial\ \mathrm{Real}(\sigma)/\partial R > 0$ is satisfied at all points on the lines, and according to [1] the lines are all "true parts" of the stability boundaries for general three-dimensional perturbations. The dynamic stability margins are usually associated with oscillatory disturbance patterns, i.e. $\mathrm{Im}(\sigma) \neq 0$.

All the points in the stability chart have been obtained by high-order approximation to reach an accuracy of $\sim 0.1\%$. For the static stability line (Re = 0) the first-order approximation ($N = 1$) is sufficient. For $\mathrm{Re} = 10^3$ and 10^5 the required approximations are with $N = 30$ and 80, and for $\mathrm{Re} = 10^5$ even $N = 100$ does not provide this accuracy.

As mentioned above, the stability chart in Fig. 1 was constructed for $\beta = 20\beta^* = 53.6$. The numerical results show that this value is close to the critical one in the region treated. Variations of β between 50 and 75 yielded values of S_1 within less than 0.1%. For $\beta < 50$ and $\beta > 75$ the lines move to the unstable region (i.e. the values of S_1 are larger than those for $50 < \beta < 75$). This behavior may, however, change when $\mathrm{Re} > 10^5$.

Figure 1 also includes the approximation $S_1/S_2 = P_1/P_2$ for the static oscillatory stability margin, for large Prandtl and Schmidt numbers, c.f. Magen [2]. As can be seen, this line belongs to the unstable zone and deviates by about 15% from the exact solution. It can serve, however, as an upper bound.

From Fig. 1 it is concluded that the stability of a solar pond does depend on the Reynolds number Re. For the parameters $P_{1,2} = 7{,}700$, $S_{1,2} = 1.6 \times 10^{13}$, 1.8×10^{15}, the pond becomes unstable at $\mathrm{Re} = \mathrm{O}(10^4)$.

5.3. Convergence

The above results have been obtained by the Galerkin method using high-order approximations. Numerical check of convergence has shown that low-order approximations

Table 3. Convergence of the Galerkin method for finding the point Re = 333.33, $S_2 = 10^8$, $\beta = 2.68$ on the dynamic marginal stability line: values of σ with the largest real part for $S_1 = 0$ and values of S_1 and ω for Real(σ) = 0 as functions of the order (N) of the Galerkin method.

	$S_1 = 0$		$\psi = \text{Real}(\sigma) = 0$	
N	$\psi = \text{Real}(\sigma)$	$\omega = \text{Im}(\sigma)$	$S_1 \times 10^{-4}$	ω
1	−11.700720	−743.40300	89.112	−893.97
2	−4.9757223	−907.79772	77.988	−644.01
3	−1.1591280	−1088.7000	2.6593	−1088.6
4	9.7023499	−932.10407	−38.070	−932.28
5	11.757471	−812.47848	−60.566	
6	9.7175669	−721.15414	−63.245	
7	7.7076953	−864.41061	−40.495	
8	7.7413715	−790.32769	−31.233	
9	6.4389848	−727.98970	−27.124	
10	5.3335940	−833.50218	−18.572	
12	4.2962976	−732.02512		
14	3.5751033	−772.56361		
16	2.5988816	−802.92768		
18	1.8169904	−735.91962		
20	1.2200828	−764.67437		
21	0.79079267	−737.06970		
22	0.49520016	−788.01581		
23	0.17312245	−762.19392	−1.6477	
24	−0.22974818	−737.96478	2.3786	
25	−0.51394993	−783.09093		
26	−0.84915802	−760.24702		
28	−1.5517844	−779.17617		
30	−2.2892994	−795.43207		
35	−4.1231551	−756.35520		
40	−4.7062705	−1337.4277		
45	−4.7115197	−1337.4260		
50	−4.7111532	−1337.4261		
58	−4.7111688	−1337.4261	151.04	−1225.9
59	−4.7111688	−1337.4261	151.28	−1225.8

provide rather accurate results here, which are better than those obtained by intermediate-order approximations.

Mikhlin [12] has shown that the Galerkin method always converges for a sufficiently large N. For small N, however, the results may differ appreciably from the exact solution and even may be practically unacceptable.

Examine, for example, the point Re = 333.333, $S_2 = 10^8$, $S_1 = 0$, $\beta = 2.68$. This point is located on the S_2 axis and belongs to the stability region; thus one may expect Real(σ) < 0. Introduction of these parameters into Eq. (19) and use of the QR method yield the value of σ for various values of N. The results for the eigenvalue with the largest real part are listed in Table 3. It is found that for $1 \leqslant N \leqslant 3$, Real($\sigma$) < 0, but for $4 \leqslant N \leqslant 23$, Real($\sigma$) > 0. For $N > 24$ the real part of σ becomes, again, negative, and for $N = 60$ the result converges to the value $\sigma = -4.7111688 - i13337.4261$.

For this example the value of S_1 which corresponds to the stability line (Real(σ) = 0) has been calculated too. Results for various N are listed in Table 3. It is found that for $1 \leqslant N \leqslant 3$, S_1 is positive, for $4 \leqslant N \leqslant 23$, $S_1 < 0$, and for $N = 60$ the result converges to $S_1 = 1.513 \times 10^6$.

This numerical check has also shown that the necessary value of N for convergence increases with increasing Re, S_2, and S_1, and with decreasing β. As an example, for $S_1 = 10^8$, $\beta = 2.68$, convergence has been obtained at $N = 10$ for $\mathrm{Re} = 0$, at $N = 60$ for $\mathrm{Re} = 333.33$ and for $\mathrm{Re} = 10^6$ the method did not converge even at $N = 100$. For $\beta = 2.68$, $\mathrm{Re} = 0$, the values of N needed for convergence, depending on S_2, are: $\{S_2 = 10^5,\ N = 7\}$, $\{S_2 = 10^8,\ N = 12\}$, $\{S_2 = 10^{15},\ N = 16\}$. The dependence of N on β is demonstrated for $\mathrm{Re} = 0$, $S_2 = 10^{15}$ by: $\{\beta = 2.68,\ N = 16\}$, $\{\beta = 53.6,\ N = 1\}$. In this latter case, even the first approximation ($N = 1$) provides results accurate within five significant digits.

6. Discussion

The present work considers the stability of an infinite fluid layer with vertical temperature and salinity distributions subject to horizontal flow. Linear stability analysis, using three-dimensional perturbations, yields an eigenvalue problem, the operator of which is not self-adjoint. Therefore the stability parameter σ is generally complex ($\sigma = \psi + \mathrm{i}\omega$, $\omega \neq 0$) and the corresponding motion is oscillatory, except for the case of static monotonic instability ($\mathrm{Re} = 0$) with small ($\approx 10^3$) or negative Rayleigh numbers S_1 and S_2.

The stability chart has been obtained by a combination of a general Nth-order Galerkin method and the continuation method. It is noted that the Galerkin method may use "orthogonal functions", as well as other complete sequences of functions. Furthermore, Orszag [4] pointed out that a polynomial expansion leads to a faster convergence than an expansion by "orthogonal functions". However, he solved a single Orr-Sommerfeld equation only. In the present work three simultaneous equations had to be solved. In this case the use of the orthogonal functions leads to a simple form of the $3N \times 3N$ characteristic matrix, and to a further simplification by reduction to a $N \times N$ matrix, saving computer time and memory space.

The method developed here was applied to an example with a parabolic velocity distribution and linear vertical temperature and salinity profiles. The stability chart in the Rayleigh-numbers plane has been found for the region relevant to solar ponds. The numerical results show that the curves of dynamic stability ($\mathrm{Re} > 0$) are quite close to the statical stability ($\mathrm{Re} = 0$) margin for Reynolds numbers which are not too large ($\mathrm{Re} < 10^5$). From these results it can be deduced that the stability of a solar pond depends on Re and that an instability would occur when Re is larger than $O(10^4)$.

The numerical results also show that for small values of the Rayleigh numbers S_1, S_2 ($\approx 10^3 - 10^4$) the value of the wave number β associated with the instability is near to 2.7 (a value corresponding to statical monotonic instability), but for large values of S_1 and S_2 the most dangerous β is about 50.

Appendix A. Differentiation of an eigenvalue with respect to a parameter

Consider a Hilbert space R^n with the ordinary inner product $\langle u \cdot v \rangle$, $\forall u,\ v \in R^n$. In this space we define two generalized eigen-problems adjoint to one-another,

$$\begin{aligned} &Lx = \sigma Mx, \quad L^*x^* = \bar{\sigma} M^* x^*, \\ &\langle u \cdot Lv \rangle = \langle L^* u \cdot v \rangle, \quad \langle u \cdot Mv \rangle = \langle M^* u \cdot v \rangle, \quad \forall u,\ v \in R^n, \end{aligned} \tag{A-1}$$

where L, L^* and M, M^* are adjoint linear operators, x, x^* are the eigenvectors and σ is the eigenvalue; M and M^* are not singular operators.

Suppose that L and M depend on the parameter ξ and the derivatives $\mathrm{d}L/\mathrm{d}\xi$ and $\mathrm{d}M/\mathrm{d}\xi$ can be defined in the usual way. Changing the parameter ξ causes a variation of σ and the derivative $\mathrm{d}\sigma/\mathrm{d}\xi$ is sought. It has been shown (e.g. Wasserstrom [3] and Magen [2]), that if the eigenvalue σ is simple (not double), the value of $\mathrm{d}\sigma/\mathrm{d}\xi$ is given by the following form:

$$\frac{\mathrm{d}\sigma}{\mathrm{d}\xi} = \left(\left\langle x^* \cdot \frac{\mathrm{d}L}{\mathrm{d}\xi} x \right\rangle - \sigma \left\langle x^* \cdot \frac{\mathrm{d}M}{\mathrm{d}\xi} x \right\rangle \right) / \langle x^* \cdot Mx \rangle . \tag{A-2}$$

This result can be expanded for a general Hilbert space with the single limiting condition $\langle x^* \cdot Mx \rangle \neq 0$, where x^* and x correspond to the same *simple* eigenvalue. It is noted that the last condition is generally satisfied and in the case of R^n it is always satisfied. For the case of double eigenvalues, Eq. (A,2) may not hold.

Equations (A.2) and (19) are used to obtain the following derivatives:

$$\frac{\partial S_{1c}}{\partial S_2} = \frac{\left\langle x^* \cdot \left[\Lambda + P_1 \sigma I + \mathrm{i} P_1 R\Gamma \right) \cdot \left(\Lambda + P_2 \sigma I + \mathrm{i} P_2 R\Gamma \right)^{-1} x \right] \rangle}{\langle x^* \cdot x \rangle}, \tag{A-3}$$

$$\begin{aligned} \frac{\partial S_{1c}}{\partial \sigma} = & \left\langle x^* \cdot \left\{ P_1 \left[S_2 \left(\Lambda + P_2 \sigma I + \mathrm{i} P_2 R\Gamma \right)^{-1} + \beta^{-2} \left(\eta^T \right)^{-1} \cdot \left(\Lambda_3 + \sigma I + \mathrm{i} R\Gamma_3 \right) \cdot \eta^{-1} \right] \right\rangle \\ & + \left(\Lambda + P_1 \sigma I + \mathrm{i} P_1 R\Gamma \right) \\ & \times \left\langle \left[-S_2 P_2 \left(\Lambda + P_2 \sigma I + \mathrm{i} P_2 R\Gamma \right)^{-2} + \beta^{-2} \left(\eta^T \right)^{-1} \cdot \eta^{-1} \right] \right\} \cdot x \Big\rangle \\ & / \langle x^* \cdot x \rangle, \end{aligned} \tag{A-4}$$

$$\frac{\partial S_{1c}}{\partial \omega} = \mathrm{i} \frac{\partial S_{1c}}{\partial \sigma} \Big|_{\sigma = \mathrm{i}\omega}, \tag{A-5}$$

where x is the eigenvector of matrix (19) and x^* is the eigenvector of the adjoint one. In deriving Eq. (A-4) use has been made of the relationship $\mathrm{d}(L^{-1})/\mathrm{d}\xi = -L^{-1} \cdot \mathrm{d}L/\mathrm{d}\xi \cdot L^{-1}$.

Proof of Eq. (A.2)

Suppose that σ is a simple eigenvalue of Eq. (A-1).Let us differentiate the first of Eqs. (A-1) with respect to the parameter ξ:

$$\frac{\mathrm{d}L}{\mathrm{d}\xi} x + L \frac{\mathrm{d}x}{\mathrm{d}\xi} = \frac{\mathrm{d}\sigma}{\mathrm{d}\xi} Mx + \sigma \frac{\mathrm{d}M}{\mathrm{d}\xi} x + \sigma M \frac{\mathrm{d}x}{\mathrm{d}\xi}. \tag{A-6}$$

The inner product of x^* with Eq. (A-7) yields

$$\left\langle x^* \cdot \frac{\mathrm{d}L}{\mathrm{d}\xi} x \right\rangle + \left\langle x^* \cdot L \frac{\mathrm{d}x}{\mathrm{d}\xi} \right\rangle = \frac{\mathrm{d}\sigma}{\mathrm{d}\xi} \langle x^* \cdot Mx \rangle + \sigma \left\langle x^* \cdot \frac{\mathrm{d}M}{\mathrm{d}\xi} x \right\rangle + \sigma \left\langle x^* \cdot M \frac{\mathrm{d}x}{\mathrm{d}\xi} \right\rangle . \tag{A-8}$$

The following chain of equations is formally obtained from the definition:

$$\left\langle x^* \cdot L \frac{\mathrm{d}x}{\mathrm{d}\xi} \right\rangle = \left\langle L^* x^* \cdot \frac{\mathrm{d}x}{\mathrm{d}\xi} \right\rangle = \left\langle \bar{\sigma} M^* x^* \cdot \frac{\mathrm{d}x}{\mathrm{d}\xi} \right\rangle = \sigma \left\langle M^* x^* \cdot \frac{\mathrm{d}x}{\mathrm{d}\xi} \right\rangle = \sigma \left\langle x^* \cdot M \frac{\mathrm{d}x}{\mathrm{d}\xi} \right\rangle . \tag{A-8}$$

Substitution of this last result into Eq. (A-7) leads to Eq. (A-2).

References

[1] M. Magen, D. Pnueli and Y. Zvirin, The stability chart of parallel shear flows with double diffusive processes – general properties, *J. Eng. Math.* 19 (1985) 175–187.

[2] M. Magen, Thermohaline stability with general horizontal flows. D.Sc. thesis, Technion, Haifa, Israel (1983).

[3] E. Wasserstrom, Numerical solution by the continuation method, *SIAM Review* 15 (1973) 89–119.

[4] S.A. Orszag, Accurate solution of the Orr-Sommerfeld stability equation, *J. Fluid Mech.* 50 (1971) 689–703.

[5] C.E. Grosch and H. Salwen, The stability of steady and time-dependent plane Poiseuille flow, *J. Fluid Mech.* 34 (1968) 177–205.

[6] H. Weinberger, The physics of the solar pond, *Solar Energy* 8 (1964) 45–56.

[7] A. Rabl and C.E. Nielsen, Solar ponds for space heating, *Solar Energy* 17 (1975) 1–12.

[8] F. Zangrando and H.C. Bryant, A salt gradient solar pond, *Solar Age* 3 (1978) 21–36.

[9] D.L. Harris and W.H. Reid, On orthogonal functions which satisfy four boundary conditions. *Astrophys. J. Suppl. Ser.* 3 (1958) 429–452.

[10] D.A. Nield, The thermohaline Rayleigh-Jeffreys problem, *J. Fluid Mech.* 29 (1967) 545–558.

[11] J.H. Wilkinson, *The Algebraic Eigenvalue Problem*, Oxford Univ. Press (1965).

[12] S.G. Mikhlin, *Direct Methods in Mathematical Physics* (in Russian), Gos. Izd. Technico-Teor. Lit., Moskwa – Leningrad (1950).